

Resolving IRAS 09111–1007 at 350 μm : a different path to ULIRG formation?

Sophia A. Khan,^{1,2*} Dominic J. Benford,² David L. Clements,¹ S. Harvey Moseley,² Richard A. Shafer² and Timothy J. Sumner¹

¹Imperial College London, Blackett Laboratory, Prince Consort Road, London SW7 2AZ

²Infrared Astrophysics Branch, Code 685, NASA/GSFC, Greenbelt, MD 20771, USA

Accepted 2005 January 25. Received 2005 January 24; in original form 2004 November 23

ABSTRACT

We have resolved the ultraluminous infrared galaxy (ULIRG) IRAS 09111–1007 with the new 350- μm -optimized Second Generation Submillimeter High Angular Resolution Camera (SHARC II), and present the first submillimetre fluxes and images for the system. IRAS 09111–1007 comprises two interacting luminous infrared galaxies (LIRGs) with a projected nuclear separation of $39 h_{71}^{-1}$ kpc. The western galaxy is roughly four times more luminous in the submillimetre than its eastern counterpart. It is an extremely bright LIRG with an active galactic nucleus (AGN). The classification of the eastern source is uncertain: it could be a Seyfert 2 galaxy or a LINER. We highlight IRAS 09111–1007 as a system that necessitates further study: a double AGN ULIRG whose molecular gas content differs from that of other widely separated pairs, and whose ULIRG phase might not be explained by current multiple-merger and/or final-stage ULIRG scenarios.

Key words: galaxies: individual: IRAS 09111–1007 – galaxies: interactions – galaxies: Seyfert – galaxies: starburst – infrared: galaxies.

1 INTRODUCTION

Amongst the first results of extragalactic mid-infrared astronomy was the discovery of a small number of galaxies that emit the bulk of their bolometric luminosity in the infrared (Low & Kleinmann 1968; Kleinmann & Low 1970a,b). The *InfraRed Astronomical Satellite*, *IRAS*, detected large numbers of these ultraluminous infrared galaxies (ULIRGs) (Soifer et al. 1984; Joseph & Wright 1985; Soifer, Neugebauer & Houck 1987) with quasar-like luminosities of $L_{\text{IR}}(8\text{--}1000\ \mu\text{m}) > 10^{12} L_{\odot}$. There is still debate as to the nature of the far-infrared power source in these galaxies: is the immense thermal energy driven by a dominant starburst, a dominant active galactic nucleus (AGN) or some combination of the two? These low-redshift *IRAS*-selected ULIRGs are expected to be the counterparts to the high-redshift ($z > 1$) SCUBA sources (see e.g. Smail et al. 1998; Blain et al. 2002; Webb et al. 2003; Chapman et al. 2003).

Most ULIRG systems have been shown to be disturbed, interacting or merging in some way when the separation of nuclei is less than 10 kpc (Sanders et al. 1988; Clements et al. 1996; Murphy et al. 1996; Farrah et al. 2001). The nature of widely separated ULIRG systems is less clear (Dinh-V-Trung et al. 2001; Meusinger et al. 2001): are the components of the ULIRG (supposedly the end phase of the galactic interaction) beginning another

merger or is the ULIRG a result of a multiple-merger event (Borne et al. 2000)? This latter scenario is possible in widely separated ULIRGs with resolved double nuclei, but might not apply to the ULIRG system IRAS 09111–1007, which consists of two widely spaced but interacting luminous infrared galaxies (LIRGs), each with a single nucleus. The two LIRGs have a projected separation of $39 h_{71}^{-1}$ kpc and a velocity difference of $425\ \text{km s}^{-1}$ (Duc, Mirabel & Maza 1997). In this Letter we present 350- μm resolved images and fluxes for IRAS 09111–1007. We model the far-infrared dust emission to constrain the nature of the interaction.

2 OBSERVATIONS AND DATA REDUCTION

The data were taken using the Second Generation Submillimeter High Angular Resolution Camera (SHARC II) at the Caltech Submillimeter Observatory (CSO) on Mauna Kea, Hawai'i, in 2004 January and March. SHARC II is a 350- μm -optimized camera (Dowell et al. 2003) built around a 12×32 element close-packed bolometer array (Moseley et al. 2004). It achieves a point-source sensitivity of $\sim 1\ \text{Jy Hz}^{-1/2}$ in good weather. The 384 pixels of the SHARC II array image a region of around $1.0 \times 2.5\ \text{arcmin}^2$. Its filled absorber array provides instantaneous imaging of the entire field of view, sampled at roughly 2.5 pixels per nominal beam area. The beam profile was measured on known compact sources, and was verified to be within 5 per cent of the diffraction-limited beamwidth of 8.5 arcsec.

*E-mail: khan@stars.gsfc.nasa.gov

For these data the in-band zenith atmospheric opacity ($\tau_{350\ \mu\text{m}}$) ranged from 1.1 to 1.3, corresponding to a zenith transmission of around 30 per cent. Our observations were centred on the eastern source of the pair, at position RA = $09^{\text{h}}13^{\text{m}}38^{\text{s}}.6$, Dec. = $-10^{\circ}19'20''$ (J2000).

In the submillimetre, emission from the atmosphere dominates the signal read out by the bolometers. In order to detect the faint celestial sources it is necessary to remove this emission. The sky signal, however, is largely correlated between pixels. At any moment in time, every pair of pixels can be used as a ‘signal’ beam and a ‘reference’ beam. Additionally, the telescope is moved such that each position on the sky can be viewed by many detectors at different times. This introduces a self-consistent self-calibration of all pixels compared with all others. A Lissajous scan pattern is used to ensure that the area on the sky is well covered and has substantial redundancy of observing.

The data were reduced using the standard CSO reduction software, CRUSH (Kovács, in preparation). This software implements a self-consistent least-squares algorithm to solve for the celestial emission, taking into account instrumental and atmospheric contributions to the signal. All observations were taken using the Dish Surface Optimization System (Leong et al. 2003), which corrects for the primary mirror deformation as a function of zenith angle, to improve the telescope efficiency and the pointing.

The sky map was calibrated with a point-spread function based on all point-source observations (Callisto, Ceres and Arp 220) through the observing period at similar elevations. An oversampled χ^2 fit was used to determine the position of the source and the flux per beam. The processed image is shown in Fig. 1.

3 RESULTS

We are able to resolve the IRAS 09111–1007 system and obtain 350- μm fluxes and positions. An absolute pointing offset of 2.0 arcsec ($\Delta\alpha = 1.0$ arcsec, $\Delta\delta = 1.7$ arcsec) from the Two Micron All Sky Survey (2MASS) positions was attributed to a pointing error (due to the imprecise absolute pointing knowledge of the CSO) and removed from the SHARC II image presented in this Letter.

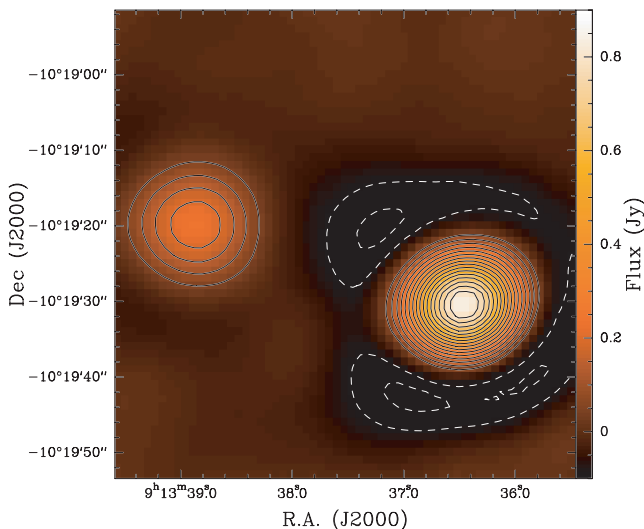


Figure 1. 350- μm continuum emission map of IRAS 09111–1007 taken with SHARC II. The contours are at levels of $50\ \text{mJy beam}^{-1}$ (dashed contours are negative and are an artefact of data reduction).

The brighter LIRG, that which contributes ≈ 79 per cent of the total system 350- μm emission, is known as the ‘western source’ or IRAS 09111–1007W for the purposes of this Letter. The eastern LIRG is called the ‘eastern source’ or IRAS 09111–1007E. Together they form the ‘ULIRG system’. Fig. 2 shows the resolved components of IRAS 09111–1007 imaged with the Digitized Sky Survey (DSS), 2MASS and *IRAS* (HIRES processed; Surace, Sanders & Mazzarella 2004) respectively. The 350- μm fluxes for each component are presented in Table 1. The signal-to-noise ratio in the detection is 89 for the western source and 29 for the eastern source. The western source is roughly four times more luminous in the submillimetre than its eastern counterpart.

4 SPECTRAL ENERGY DISTRIBUTION MODELLING

4.1 Dust temperature blackbody fitting

A modified blackbody is used to model the total dust emission of the IRAS 09111–1007 system, specifically

$$F_{\nu} = (M_{\text{dust}}/D^2)\kappa(\lambda)B_{\nu}(\lambda, T_{\text{dust}}), \quad (1)$$

where B_{ν} is the Planck function, κ the mass absorption coefficient of the dust [$\kappa(\lambda) \propto \lambda^{-\beta}$, see Dwek 2004], T_{dust} and M_{dust} the equilibrium dust temperature and mass respectively, and D the distance of the galaxy. For the distance we use *WMAP* cosmology [$H_0 = 71\ \text{km s}^{-1}\ \text{Mpc}^{-1}$, $\Omega_{\text{m}} = 0.27$ and $\Omega_{\Lambda} = 0.73$ (Bennett et al. 2003)].

In order to constrain better the spectral energy distribution (SED) of each component, we determined the ratio of the fluxes of the two components at 60 μm . Beginning with the *IRAS* 60- μm HIRES-processed image of Surace et al. (2004), we sliced along the axis of the known 350- μm sources. A pair of Gaussian intensity functions were fitted to the measured flux along this slice, constraining them to have the same width and a fixed spacing as determined at 350 μm (see Fig. 3). The remaining four free parameters (one position, the width, and the two intensities) are then well-constrained, with the flux ratio being 4.9 ± 0.8 (the total system flux as measured by *IRAS* is still valid, since the *IRAS* fluxes are derived with an aperture large compared with the source separation). The ratio derived from the 350- μm measurement is 3.7 ± 1.1 . Alternatively, the fraction of the flux from the western source is 83 ± 3 per cent at 60 μm and 79 ± 16 per cent at 350 μm , an entirely consistent measurement. The ratio of 79 per cent is accurate enough for the fits that follow.

χ^2 minimization, results summarized in Table 2 determined the best-fitting emissivity index (β) and corresponding single-fit dust temperature for the system using the SHARC II 350- μm flux with the 60- and 100- μm *IRAS* fluxes derived by Surace et al. (2004) (the 100- μm flux was used as the normalization). The best-fitting was $\beta = 1.9 \pm 0.1$, $T = 31 \pm 1$ K, and is shown in Fig. 4. We also modelled both the western and eastern sources assuming that the *IRAS* fluxes are distributed in the same way as the 350- μm emission. Dust masses were calculated assuming that the 100- μm mass absorption coefficient, κ_{100} , is $40\ \text{cm}^2\ \text{g}^{-1}$ (Draine & Lee 1984).

With only two independent colours we cannot constrain the cold and warm dust masses and simultaneously fit the dust temperatures in a two-temperature model. Using $\beta = 2$ (as in Dunne & Eales 2001), if we assume equal amounts of cold and warm dust in the system we get best-fitting temperatures of $T_{\text{cold}} = 26 \pm 5$ K and $T_{\text{warm}} = 32 \pm 2$ K. If we adopt a dust mass distribution typical of the highest luminosity galaxies from the SCUBA Local Universe Galaxy Survey (SLUGS), as given in Dunne & Eales (2001), we get

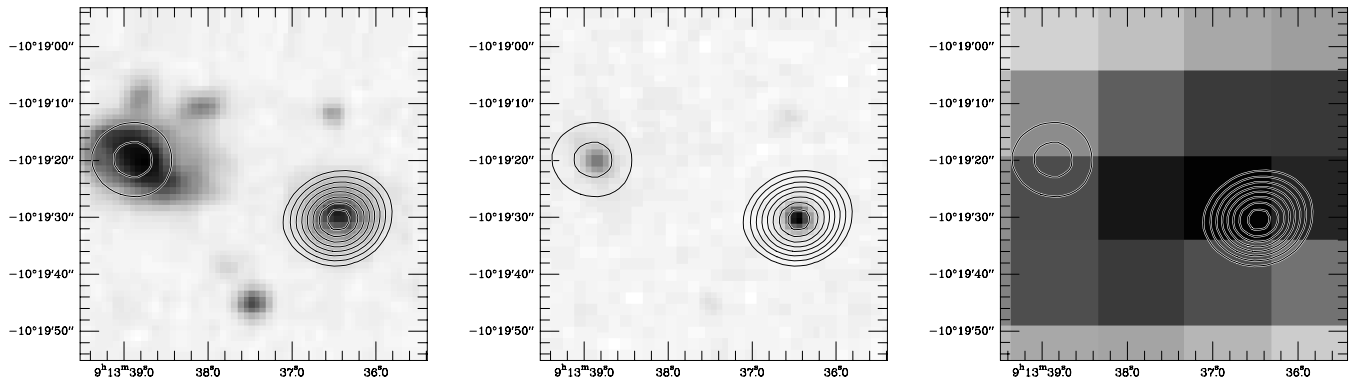


Figure 2. DSS optical, 2MASS K_s and $IRAS$ 60- μm images of IRAS 09111–1007, with 350- μm contours overlaid on each (at levels of 100 mJy beam $^{-1}$).

Table 1. Coordinates, 350- μm fluxes, luminosities and star formation rates for the system and both components of IRAS 09111–1007 ($IRAS$ fluxes from Surace et al. 2004). The far-infrared (40–500 μm) and infrared (8–1000 μm) luminosities are derived as follows: $L_{\text{FIR:SED}}$ is computed from the best-fitting single-temperature SED; $L_{\text{FIR:IRAS}}$ and L_{IR} are calculated using the standard relations from Fullmer & Lonsdale (1989) and Sanders & Mirabel (1996) respectively. Note that the pair positions given in both NED and Surace et al. (2004) are swapped.

Name	Coordinates (J2000)	350- μm flux (Jy)	$\log(L_{\text{FIR:SED}})$ (L_{\odot})	$\log(L_{\text{FIR:IRAS}})$ (L_{\odot})	$\log(L_{\text{IR}})$ (L_{\odot})	SFR ($M_{\odot} \text{ yr}^{-1}$)
IRAS 09111–1007			11.91	11.86	12.09	81
IRAS 09111–1007W	09 ^h 13 ^m 36 ^s .4 – 10° 19′ 31″.8	0.85 ± 0.13	11.80	11.75	11.98	63
IRAS 09111–1007E	09 ^h 13 ^m 38 ^s .8 – 10° 19′ 21″.5	0.23 ± 0.04	11.25	11.20	11.43	18

Table 2. Best-fitting SED parameters: β , temperature and dust mass for the IRAS 09111–1007 system and components, with corresponding estimated 1σ uncertainties.

Model	Source	β	T_{dust} (K)	M_{dust} ($10^6 M_{\odot}$)
Single-temperature	System	1.9 ± 0.1	31 ± 1	220 $^{+30}_{-20}$
	Western source	1.9 ± 0.1	31 ± 1	170 $^{+30}_{-20}$
	Eastern source	1.9 ± 0.1	31 ± 1	50 $^{+10}_{-10}$
Two-temperature $M_{\text{cold}}/M_{\text{warm}} = 1$	System	2.0 (fixed)	32 ± 2 26 ± 5	300 $^{+190}_{-110}$
	System	2.0 (fixed)	36 ± 3 29 ± 1	280 $^{+70}_{-50}$
Single-temperature	System	n/a	30 ± 1	250 $^{+30}_{-30}$
DL dust model	Western source	n/a	30 ± 1	200 $^{+30}_{-30}$
	Eastern source	n/a	30 ± 1	60 $^{+10}_{-10}$

a ratio $M_{\text{cold}}/M_{\text{warm}} = 11$. The best-fitting values are then $T_{\text{cold}} = 29 \pm 1$ K, $T_{\text{warm}} = 36 \pm 3$ K.

As an alternative to these approaches, we also used a more physically based dust grain model [the single-temperature DL dust model (Draine & Lee 1984; Laor & Draine 1993)], an equal mixture of silicates and graphites with κ_{100} of 31 and 54 $\text{cm}^2 \text{g}^{-1}$ for the silicate and graphite grains respectively. In this case, the best-fitting temperature of the system was 30 ± 1 K.

The dust temperature of ~ 31 K is within 1.5σ of the average temperature of 38 ± 6 K from the previous 350- μm LIRG study by Benford (1999), with the first SHARC camera (although that survey did not include any widely separated LIRG systems). The result that

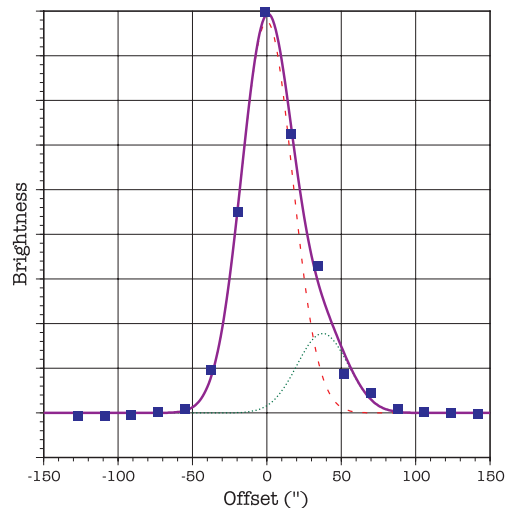


Figure 3. Fit to the spatial variation in intensity for the HIRES-processed $IRAS$ 60- μm image, cut through both galaxies.

the 60- μm dust is distributed in very similar ratios to the 350- μm dust (Fig. 3) is responsible for the identical SED temperatures for both components.

4.2 Ratio of molecular gas to dust

The molecular gas mass in the western source is $2.3 \times 10^{10} M_{\odot}$ (Mirabel et al. 1990). The dust mass of the western source is derived from the best-fitting SED to give molecular gas-to-dust ratios of 140 and 120 for the single-temperature and DL dust models respectively. In the absence of 21-cm H I observations, this value is a lower limit on the total (molecular + atomic) gas-to-dust ratio.

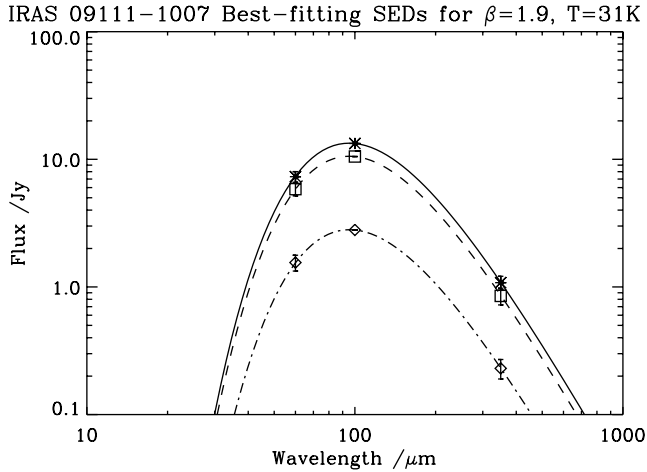


Figure 4. Single-temperature best-fitting SED for the western source (dashed), the eastern source (dot-dashed) and the IRAS 09111–1007 system (solid: $\beta = 1.9$, $T = 31$ K).

The 8–1000 μm luminosity (L_{IR} , see Table 1) gives a value for the western source infrared luminosity-to- H_2 mass ratio [$L_{\text{IR}}/M(\text{H}_2)$ – the star formation efficiency] of $42 L_{\odot} M_{\odot}^{-1}$. The molecular gas-to-dust and infrared luminosity-to- H_2 mass ratios are consistent with values for the highest luminosity SLUGS galaxies (Dunne et al. 2000).

Dinh-V-Trung et al. (2001) studied six widely separated (>20 kpc) ULIRG systems in the complete 1-Jy sample of Kim & Sanders (1998). In their sample, the molecular gas was concentrated in the dominant source of the far-infrared emission. Although the western source of IRAS 09111–1007 is gas-rich, the eastern source, by virtue of the amount of dust, is unlikely to be gas-poor. This would make this system different from their wide-pair ULIRG sample.

4.3 Star formation rate

The system and component luminosities (see Table 1) show that the two components form a ULIRG system, although neither is a ULIRG individually. The star formation rate in Table 1 uses the SED-derived far-infrared luminosities and the relation of Thronson & Telesco (1986):

$$\text{SFR} \sim \Psi 10^{-10} \left(\frac{L_{\text{FIR}}}{L_{\odot}} \right) M_{\odot} \text{ yr}^{-1} \quad (2)$$

assuming $\Psi = 1$ (typical values of Ψ are 0.8–2.1).

5 DISCUSSION

5.1 Source characterization

The optical image from the DSS (Fig. 2, left) shows the disturbed morphology of the eastern source. In the 2MASS K_s -band image (Fig. 2, centre) the western source is slightly more luminous than the eastern, a trait even more prominent in the submillimetre (Fig. 1). Merger models such as Barnes & Hernquist (1991) predict gas and dust to be concentrated in the galaxy centre as the ULIRG interaction condenses large amounts of the interstellar medium into the nuclear region.

Line ratios from Duc et al. (1997) classify the western source as a Seyfert 2. Dudley (1999) found prominent polycyclic aromatic

hydrocarbon features in the 8–13 μm dust emission spectra – indicative of a starburst. The eastern source is either a Seyfert 2 or a LINER galaxy (Duc et al. 1997), while Gonçalves, Véron-Cetty & Véron (1999) also found evidence for a starburst. Neither of the two sources in the IRAS 09111–1007 system were detected in the *ROSAT* All-Sky Survey. A non-detection in the *ROSAT* band does not necessarily mean that a source is intrinsically weak, since the soft X-ray band is sensitive to X-ray absorption, which is common in AGN.

5.2 Merging stage

Without additional submillimetre data, we are unable to constrain the relative temperatures and masses of the cold and warm dust components. Whether the dust temperature of the system is related to the stage of merging is not clear. Mazzarella, Bothun & Boroson (1991) found an increase in warm dust temperature with merging stage, although Klaas et al. (2001) argued that the cold dust temperature would increase as well. The wide separation of the pair would suggest that IRAS 09111–1007 is at the beginning of a merger, a notion supported by the value of the infrared luminosity-to- H_2 mass ratio, which falls within a region of $L_{\text{IR}}/M(\text{H}_2)$ versus L_{IR} space that is common for early merging systems (Sanders, Scoville & Soifer 1991).

5.3 Widely spaced ULIRG pairs

Unlike the wide-pair sample of Xu & Sulentic (1991), *both* components are enhanced in the far-infrared. With a velocity difference of 425 km s^{-1} (Duc et al. 1997) and a projected separation of $39 h_{71}^{-1}$ kpc, Monte Carlo simulations give the probability of the pair being bound as 0.88 (Schweizer 1987).

Although widely separated ULIRG pairs are not uncommon, the nature of their interaction is still uncertain. Murphy et al. (1996) postulated the presence of a third nucleus in widely separated pairs, although no double nucleus has been detected in either component of IRAS 09111–1007. The galaxies were shown to be unresolved at 0.5-arcsec resolution in a 6-cm search by Crawford et al. (1996). However, the non-detection of a double nucleus cannot rule out a multiple merger, since the time-scale of nuclei coalescence is short (Surace, Sanders & Evans 2000; Meusinger et al. 2001). In multiple-approach merger models (e.g. Dubinski, Mihos & Hernquist 1999) the merging process is a series of encounters where bound components approach and separate. A previous encounter may have triggered the starburst/AGN in the system. High-resolution optical imaging (Borne et al. 2000) could decide between these scenarios by either detecting multiple nuclei or confirming single nuclei. High-resolution CO imaging would be needed to detect whether gas has been disturbed by a previous phase of the merging event (Mihos & Hernquist 1996).

6 CONCLUSIONS

We have resolved the widely separated ULIRG system of IRAS 09111–1007 with the SHARC II detector at 350 μm . This system comprises two LIRGs with a projected separation of $39 h_{71}^{-1}$ kpc, or around two optical diameters. The western component dominates the far-infrared flux at both 60 and 350 μm , carrying 79 per cent of the total system luminosity. Although the luminosity of the system is large, our fluxes suggest a dust temperature of 31 K for this system, with both components at the same temperature to within the sensitivity of this measurement. The wide separation and the value

of the infrared luminosity-to- H_2 mass ratio suggest that the pair are at an early stage of interaction. However, the high luminosity of the system ($L_{\text{IR}} = 1.2 \times 10^{12} L_{\odot}$) would be unusual for such a stage, unless the components had experienced a previous merger or interaction. A high-resolution optical search for multiple nuclei within each component is needed. Their absence could indicate that the double AGN–LIRG system of IRAS 09111–1007, and perhaps other widely spaced ULIRG pairs, might be unexplained by current theories of ULIRG formation and evolution.

ACKNOWLEDGMENTS

This research has made use of the NASA/IPAC Extragalactic Data base (NED), which is operated by the Jet Propulsion Laboratory under contract with NASA. The optical image is taken from photographic data obtained using the UK Schmidt Telescope. The Caltech Submillimeter Observatory is supported by NSF contract AST-0229008. We thank the anonymous referee for their insightful and careful comments. We are very grateful to Pierre-Alain Duc for providing clarification and additional spectroscopic data for the system, to Jason Surace for providing his HIRES-processed *IRAS* images, to Eli Dwek for SED discussion and the DL dust model, and to Rick Arendt for invaluable IDL data analysis advice. We extend our thanks to Tom Phillips and the CSO for our observing time and support during our runs, to Hiroshige Yoshida for undertaking heterodyne observations on our behalf, and to Darren Dowell, Attila Kovács and Colin Borys for observation and instrument assistance and support with data analysis.

REFERENCES

Barnes J. E., Hernquist L. E., 1991, *ApJ*, 370, L65
 Benford D. J., 1999, PhD thesis, California Institute of Technology
 Bennett C. L. et al., 2003, *ApJS*, 148, 1
 Blain A. W., Smail I., Ivison R. J., Kneib J.-P., Frayer D. T., 2002, *Phys. Rep.*, 369, 111
 Borne K. D., Bushouse H., Lucas R. A., Colina L., 2000, *ApJ*, 529, L77
 Chapman S. C., Blain A. W., Ivison R. J., Smail I. R., 2003, *Nat*, 422, 695
 Clements D. L., Sutherland W. J., McMahon R. G., Saunders W., 1996, *MNRAS*, 279, 477
 Crawford T., Marr J., Partridge B., Strauss M. A., 1996, *ApJ*, 460, 225
 Dinh-V-Trung, Lo K. Y., Kim D.-C., Gao Y., Gruendl R. A., 2001, *ApJ*, 556, 141

Dowell C. D. et al., 2003, *Proc. SPIE*, 4855, 73
 Draine B. T., Lee H. M., 1984, *ApJ*, 285, 89
 Dubinski J., Mihos J. C., Hernquist L., 1999, *ApJ*, 526, 607
 Duc P.-A., Mirabel I. F., Maza J., 1997, *A&AS*, 124, 533
 Dudley C. C., 1999, *MNRAS*, 307, 553
 Dunne L., Eales S. A., 2001, *MNRAS*, 327, 697
 Dunne L., Eales S., Edmunds M., Ivison R., Alexander P., Clements D. L., 2000, *MNRAS*, 315, 115
 Dwek E., 2004, *ApJ*, 607, 848
 Farrah D. et al., 2001, *MNRAS*, 326, 1333
 Fullmer L., Lonsdale C. J., 1989, JPL D-1932, Version 2, Part No. 3
 Gonçalves A. C., Véron-Cetty M. P., Véron P., 1999, *A&AS*, 135, 437
 Joseph R. D., Wright G. S., 1985, *MNRAS*, 214, 87
 Kim D.-C., Sanders D. B., 1998, *ApJS*, 119, 41
 Klaas U. et al., 2001, *A&A*, 379, 823
 Kleinmann D. E., Low F. J., 1970a, *ApJ*, 159, L165
 Kleinmann D. E., Low F. J., 1970b, *ApJ*, 161, L203
 Laor A., Draine B. T., 1993, *ApJ*, 402, 441
 Leong M., 2003, <http://www.cso.caltech.edu/dsos/DSOSAMOSpaper.pdf>
 Low J., Kleinmann D. E., 1968, *AJ*, 73, 868
 Mazzarella J. M., Bothun G. D., Boroson T. A., 1991, *ApJ*, 101, 2034
 Meusinger H., Stecklum B., Theis C., Brunzendorf J., 2001, *A&A*, 379, 845
 Mihos J. C., Hernquist L., 1996, *ApJ*, 464, 641
 Mirabel I. F., Booth R. S., Johansson L. E. B., Garay G., Sanders D. B., 1990, *A&A*, 236, 327
 Moseley S. H., Allen C. A., Benford D., Dowell C. D., Harper D. A., Phillips T. G., Silverberg R. F., Staguhn J., 2004, *Nucl. Instruments Methods Phys. Res. Sec. A*, 520, 417
 Murphy T. W., Jr, Armus L., Matthews K., Soifer B. T., Mazzarella J. M., Shupe D. L., Strauss M. A., Neugebauer G., 1996, *AJ*, 111, 1025
 Sanders D. B., Mirabel I. F., 1996, *ARA&A*, 34, 749
 Sanders D. B., Soifer B. T., Elias J. H., Madore B. F., Matthews K., Neugebauer G., Scoville N. Z., 1988, *ApJ*, 325, 74
 Sanders D. B., Scoville N. Z., Soifer B. T., 1991, *ApJ*, 370, 158
 Schweizer L. Y., 1987, *ApJS*, 64, 427
 Smail I., Ivison R. J., Blain A. W., Kneib J.-P., 1998, *ApJ*, 507, L21
 Soifer B. T. et al., 1984, *ApJ*, 278, L71
 Soifer B. T., Neugebauer G., Houck J. R., 1987, *ARA&A*, 25, 187
 Surace J. A., Sanders D. B., Evans A. S., 2000, *ApJ*, 529, 170
 Surace J. A., Sanders D. B., Mazzarella J. M., 2004, *AJ*, 127, 3235
 Thronson H., Telesco C., 1986, *ApJ*, 311, 98
 Webb T. M. A., Lilly S. J., Clements D. L., Eales S., Yun M., Brodwin M., Dunne L., Gear W. K., 2003, *ApJ*, 597, 680
 Xu C., Sulentic J. W., 1991, *ApJ*, 374, 407

This paper has been typeset from a $\text{\TeX}/\text{\LaTeX}$ file prepared by the author.